Research Paper https://doi.org/10.7733/jnfcwt.2023.014

Evaluation of Effects of Impurities in Nuclear Fuel and Assembly Hardware on Radiation Source Term and Shielding

Taekyung Lee*, Dongjin Lee, Kwangsoon Choi, and Hyeongjoon Yun
KEPCO Engineering & Construction Company, Inc., 111, Daedeok-daero 989beon-gil, Yuseong-gu, Daejeon 34057, Republic of Korea

(Received October 26, 2022 / Revised November 15, 2022 / Approved December 16, 2022)

To ensure radiological safety margin in the transport and storage of spent nuclear fuel, it is crucial to perform source term and shielding analyses in advance from the perspective of conservation. When performing source term analysis on UO_2 fuel, which is mostly used in commercial nuclear power plants, uranium and oxygen are basically considered to be the initial materials of the new fuel. However, the presence of impurities in the fuel and structural materials of the fuel assembly may influence the source term and shielding analyses. The impurities could be radioactive materials or the stable materials that are activated by irradiation during reactor power operation. As measuring the impurity concentration levels in the fuel and structural materials can be challenging, publicly available information on impurity concentration levels is used as a reference in this evaluation. To assess the effect of impurities, the results of the source term and shielding analyses were compared depending on whether the assumed impurity concentration is considered. For the shielding analysis, generic cask design data developed by KEPCO-E&C was utilized.

Keywords: Spent nuclear fuel, Impurities, Source term, Shielding, Cask

*Corresponding Author.
Taekyung Lee, KEPCO Engineering & Construction Company, Inc., E-mail: tklee85@kepco-enc.com, Tel: +82-42-820-4468

ORCID

Taekyung Lee	http://orcid.org/0009-0000-7497-1844	Dongjin Lee	http://orcid.org/0009-0003-6196-3425
Kwangsoon Choi	http://orcid.org/0009-0003-0891-1802	Hyeongjoon Yun	http://orcid.org/0009-0008-5181-8239

1. Introduction

Radiation source term analysis for the spent fuel assembly applying the nominal initial compositions of UO_2 fuel and structural materials can be readily performed by using a widely used computer code such as ORIGEN module of SCALE code systems [1]. However, the determination of the impurity concentration levels for the source term analysis may be hard due to the difficulties in measurement and large uncertainties. The purpose of this evaluation is to see how much effect on the source term and shielding can occur when the conservative impurity concentration data publicly available is applied and the activation of the impurities is additionally considered. The spent fuel is transported and stored before the disposal by using casks such as transport cask, storage cask or dual-purpose cask. Therefore, the effect of the impurities considered on the shielding analysis is evaluated based on a generic cask design which was developed by KEPCO-E&C. The design data of PLUS7 fuel assembly is used for the representative model of fuel type in this evaluation.

2. Methodology

2.1 Theory and Computer Code

In the source term analysis for the spent fuel, neutrons and gammas emitted from the active fuel region are basically considered and can be easily calculated with ORIGEN. The other sources to be considered for shielding analysis are the activated structural materials and the secondary gammas. Since the secondary gammas depend not only on the fuel region but also on the shielding structures and materials, commonly used Monte Carlo transport codes such as MCNP and SCALE/MAVRIC provide a relevant calculation option to consider the secondary gammas.

The concerned impurities of the fuel assembly can be largely divided into two groups. One is present in the fuel and the other in the structural materials. The impurities assumed to be present in the fuel could be considered in the source term analysis for the active fuel using ORIGEN. For the impurities in the structural materials, additional activation analyses are required because the structural hardware regions are outside the fueled region.

For evaluating the activation of structural materials of fuel assembly, several methodologies can be considered. First of all, it is necessary to recognize that neutron flux level and energy spectrum in the assembly hardware regions (In general, axially divided into upper end fitting, gas plenum and lower end fitting) are quite different from those in the active fuel region. One of the methodologies that could be considered is to use SCALE/TRITON module which can simultaneously calculate fuel depletion and structural hardware activation with locally accurate neutron energy spectrum (if specified as an individual material to use deplete-by-flux mode in the code input). However, this approach requires much time to process transport, depletion and cross sections considering every depletion interval.

If a particular cross section library for the structural hardware activation is prepared in advance, stand-alone ORIGEN activation calculation using the activation library and the flux scaling factors provided in PNL-6906 Vol. 1 report [2] can be considered to be the most effective and reasonably accurate way. SCALE/COUPLE module can simply create the effective one-group cross section library for use with ORIGEN if a flux spectrum in the structural hardware region is available. The flux spectra in the assembly hardware regions can be obtained by neutron transport calculation.

In this evaluation, SCALE/DENOVO module was used for the transport calculation in terms of its simplicity and time efficiency. DENOVO is a three dimensional discrete-ordinates code that performs deterministic transport calculation, which means it has a great advantage of taking less time and effort than other Monte Carlo codes. DENOVO is generally used as a part of other modules in the SCALE code system such as MAVRIC and Sourcerer for different

Table 1. The range of cobalt impurity concentration in common reactor materials

Material	Cobalt concentration (ppm)
Zircaloy-2	2 – 20
Zircaloy-4	2 – 20
Inconel-718	4,694 – 10,000
Inconel X-750	300 – 10,000
Stainless steel 304	800

applications, but can also be run in stand-alone mode within MAVRIC. It could be generally expected that the flux of the regions above and below the active core would be much smaller than the flux in the active core region. However, another important factor for the activation analysis is the proportion of thermalized neutrons with large activation cross sections. It is also important that the materials such as stainless steel and Inconel are typically used for structural supports of fuel assembly. The reason why the stainless steel and Inconel are important to the activation analysis is described in the following section.

2.2 Activation and Source Terms

As the structural materials of the fuel assembly, zirconium alloy, Inconel and stainless steel are widely used. It is generally known that Zircaloy which is a representative subgroup of zirconium alloys and commonly used as cladding material contains quite low cobalt impurities. However, Inconel which is widely used as the material for top/bottom grid assembly and protective grid assembly might contain considerable cobalt impurity (mostly present as ^{59}Co) producing ^{60}Co which is a major activation source and strong gamma emitter. Also, the stainless steel used for the upper/lower end fitting could contain relatively high cobalt impurity, compared to Zircaloy material. A recent research report [3] publicly available related to the impurities in LWR fuel and structural materials provides the range of cobalt impurity concentration in common structural materials as shown in Table 1. The range of impurity concentration per

Table 2. The range of impurity concentration per each element in UO_2 fuel

Element	Concentration (ppm)	Element	Concentration (ppm)
Ag	0.1 – 25	Li	1
Al	100 – 400	Lu	0.3
Ar	0.1	Mg	60 – 200
As	3	Mn	1.7 – 200
Au	1	Mo	8 – 400
B	0.4 – 1	N	100 – 200
Ba	100	Na	20 – 400
Be	0.1	Nb	10
Bi	0.4 – 20	Ni	24 – 400
Br	5	Os	1
C	89.4 – 200	P	60
Ca	2 – 250	Pb	1 – 400
Cd	0.4 – 25	Pt	1
Ce	10	Re	1
Cl	5 – 15	Ru	1
Co	1 – 75	S	20
Cr	4 – 400	Sb	1
Cu	1 – 400	Sc	20
Dy	0.3	Se	20
Er	0.3	Si	120 – 250
Eu	0.3	Sm	0.3
F	25 – 50	Sn	1 – 400
Fe	18 – 600	Ta	10
Ga	3	Tb	0.3
Gd	0.2 – 2.5	Te	1
Ge	3	Th	10 – 500
H	1	Ti	1 – 20
Hf	10	Tl	1
Hg	1	Tm	0.3
Ho	0.3	V	3 – 400
In	1 – 2	W	2 – 100
Ir	1	Yb	0.3
K	20	Zn	20 – 400
La	10	-	-

each element in UO_2 fuel is presented in Table 2. Those impurity concentration values are based on a literature survey.

In order to briefly find out the axial variation of the neutron energy spectra for fuel assembly, stand-alone DENOVO module for forward calculation was used. PLUS7 fuel assembly data [4] considering an axial power distribution during normal operation and a typical 3-cycle burnup history was used as the reference data for the transport calculation. The standard SCALE cross section library of 252-group neutron energy based on ENDF/B-VII.1 was selected for the DENOVO calculation.

On the other hand, neutrons from decay emission sources consist of spontaneous fission, (α,n) reaction and delayed neutron emission. The delayed neutrons can be ignored for the spent fuel because they decrease very rapidly after reactor shutdown. In UO_2 fuel, oxygen is the primary source to produce (α,n) reaction due to its large amount in the fuel even if other light element impurities that might be present in the fuel are considered. The contribution of (α,n) neutron emission to total neutron intensity of the spent fuel tends to be proportional to spent fuel cooling time and inversely proportional to burnup. For ordinary spent fuels with 3-cycle irradiation, 40–60 $GWd{\cdot}MTU^{-1}$ burnup and cooling time of 10 years, the contribution of (α,n) neutron emission to total neutron intensity is generally within 2% only.

Because the neutron source intensity of typical spent fuel is dominated by spontaneous fission neutrons (mostly by curium isotopes), it can be assumed that the neutron energy spectrum of spent fuel is roughly similar to those of active fuel during power operation which is mainly composed of fast neutrons depending on Watt fission spectrum defined as:

$$p(E) = ce^{-E/a}\sinh(\sqrt{bE})$$

where

a and b = Watt spectrum parameters,

c = normalization constant.

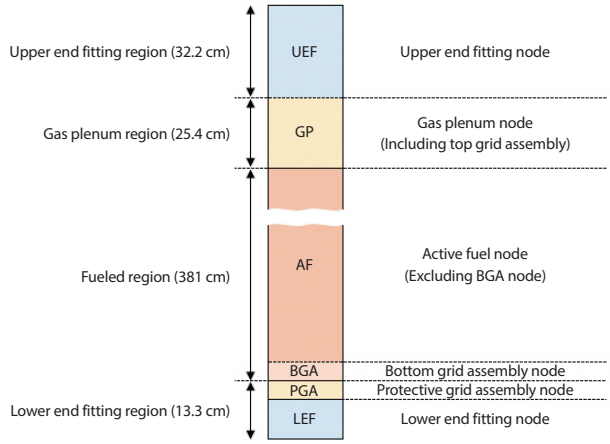

Fig. 1. Simplified model of PLUS7 fuel assembly axially divided into 6 nodes.

Strictly speaking, for induced fission, the Watt spectrum parameter depends on each fissionable nuclide and the incident neutron energy. Accordingly, the Watt spectrum parameters also differ between the spontaneous fissions of certain actinides for the spent fuel and the neutron induced fissions of major fissile nuclides. But, even if the spent fuel neutron source dominated by the spontaneous fission neutron is used for the transport calculation, a relative comparison of energy spectrum difference between the active fuel region and other assembly hardware regions could roughly show how the fast neutrons emitted by fissions are thermalized according to the axial variation of the fuel assembly.

6 nodes axially divided from the PLUS7 assembly were modeled for the DENOVO input as shown in Fig. 1, considering the material composition of each region. The 6 nodes consist of upper end fitting (UEF), gas plenum (GP), active fuel (AF), bottom grid assembly (BGA), protective grid assembly (PGA) and lower end fitting (LEF). Actually, the bottom grid assembly is installed in the active fuel region but it was separately modeled from the active fuel because it is made of Inconel which might contain substantial cobalt impurity (potentially major activation source). The materials of each node were homogenized for the transport calculation.

OASIS-STO cask design (a dry storage cask design

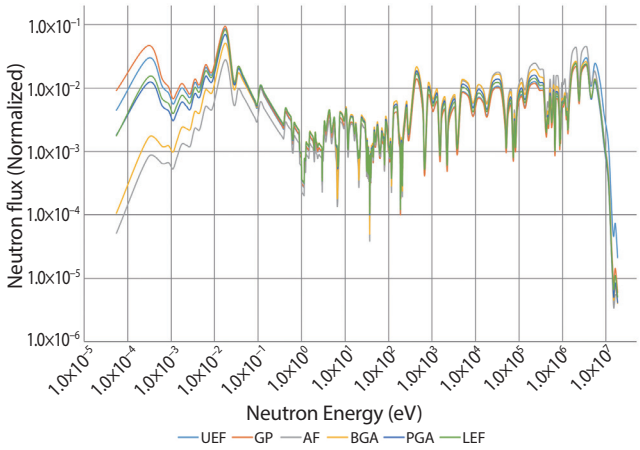

Fig. 2. Neutron energy spectrum per each node of PLUS7 fuel assembly.

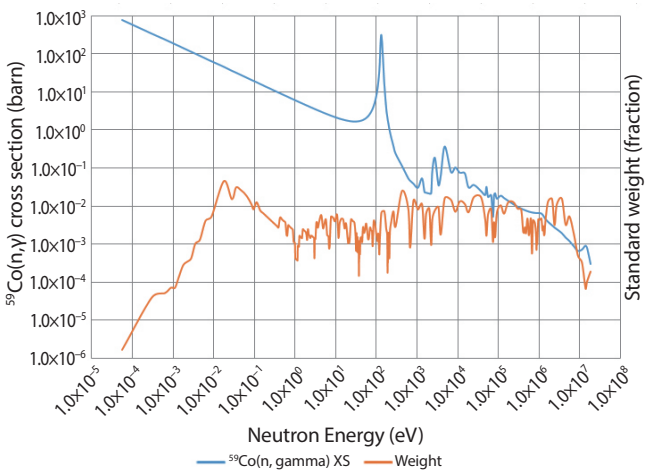

Fig. 3. ^{59}Co(n,γ) cross section and weight function of the standard SCALE library.

developed by KEPCO-E&C) which accommodates 32 spent fuel assemblies as shown in Fig. 4 was used for reference and a comparative model has been prepared by modifying the original design to have a water-filled interior and the baskets removed in order to establish the similar moderating condition with the core for normal operation.

Fig. 2 shows the neutron energy spectra of the 6 nodes of PLUS7 assembly based on the DENOVO calculation result. Each spectrum was taken from the central location of each node. Fig. 2 corresponds to the result of the assembly which is outermost from the center of the radial array of the 32 spent fuel assemblies. For reference, the outermost

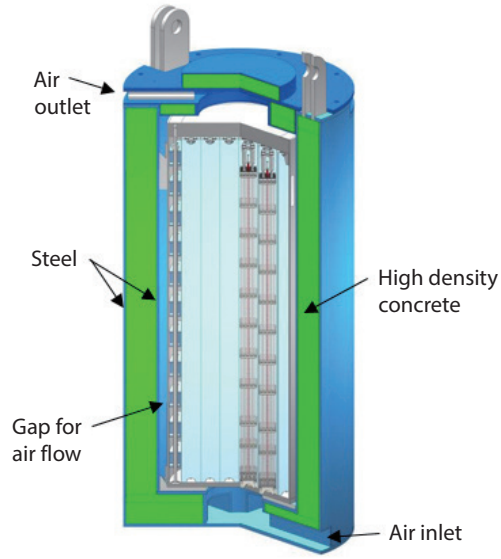

Fig. 4. OASIS-STO cask model containing a canister and 32 fuel assemblies.

assembly has a neutron spectrum composed of relatively larger fast neutron flux and smaller thermalized neutron flux in the active fuel region, compared to the assemblies located in the central part of the array. However, the proportion of thermalized neutrons in the upper end fitting of the outermost assembly is slightly larger than that in the upper end fitting of the central assembly. The difference of the proportion of thermalized neutrons in the upper end fitting between the central assembly and the outermost assembly was estimated to be within about 5%. The difference is not so large but the neutron energy spectra of the outermost assembly were considered to generate more conservative cross section data to be used for the activation analysis. For comparative reference, ^{59}Co(n,γ) cross section data and weight function of the 252-group library provided in the standard SCALE cross section libraries are shown in Fig. 3.

On the other hand, even though the upper end fitting is located farther from the active fuel rather than the gas plenum, the proportion of the thermalized neutrons in the gas plenum was estimated to be larger than that in the upper end fitting as shown in Fig. 2. It is expected that this is because ZIRLO (zirconium alloy) material is used for the fuel

Table 3. ORIGEN flux scaling factors from PNL-6906 Vol.1

Region	WE and B&W assemblies	CE assemblies	GE assemblies	Maximum
Upper end fitting	0.1	0.05	0.1	0.1
Gas plenum	0.2	0.2	0.2	0.2
Fueled region	1.0	1.0	1.0	1.0
Lower end fitting	0.2	0.2	0.15	0.2

Note: The values have an uncertainty of ±50%.

Table 4. Gamma intensities produced by the activation of cobalt impurity of 1 gram

Axial nodes	Gamma intensity ($\gamma \cdot sec^{-1}$)		Ratio to active fuel
	1.1732 MeV	1.3325 MeV	
Upper end fitting	1.73×10^{11}	1.73×10^{11}	0.50
Gas plenum (including top grid assembly)	4.57×10^{11}	4.57×10^{11}	1.32
Active fuel	3.45×10^{11}	3.46×10^{11}	1.00
Bottom grid assembly	5.68×10^{11}	5.68×10^{11}	1.65
Protective grid assembly	2.17×10^{11}	2.17×10^{11}	0.63
Lower end fitting	2.49×10^{11}	2.50×10^{11}	0.72

cladding of PLUS7 assembly and the gas plenum region includes the upper part of the fuel cladding. Meanwhile, the upper end fitting is made of SS304 only. Zirconium isotopes have relatively low absorption cross sections, compared to the stainless steel materials such as iron, chrome and nickel. And, low energy neutrons interacting with zirconium can cause both elastic and inelastic scatterings while those interacting with iron tend to be either elastically scattered or absorbed (exceptional for ^{58}Fe which could cause the inelastic scattering with low energy neutron).

The neutron flux scaling factors provided in PNL-6906 Vol. 1 report are shown in Table 3. The flux scaling factors are specified based on the three typical types of fuel assemblies. Even though the PLUS7 assembly is similar to the Combustion Engineering assemblies, the largest value for each region among the three assembly types was taken to produce conservative activation source terms in the ORIGEN calculation. The average flux level in the active fuels calculated by ORIGEN was 5.19×10^{13} $n\cdot cm^{-2}\cdot sec^{-1}$, based on the assumptions of 3.5wt% ^{235}U initial enrichment and 3-cycle burnup of 45,000 $MWd\cdot MTU^{-1}$.

The cross sections for the activation analysis were produced using COUPLE module. In order to find out the differences of the cross sections among the 6 axial nodes of the PLUS7 assembly, the activation calculations based on the energy spectrum and flux scaling factor for each node were respectively performed and the results were compared. The flux scaling factors of 1.0 and 0.2 were respectively applied to the bottom grid assembly and the protective grid assembly. The 3-cycle irradiation (375 days per cycle), refueling term of 30 days between the cycles and cooling time of 10 years after the third cycle were assumed for the ORIGEN activation calculation. Table 4 shows the major gamma source intensities (1.1732 and 1.3325 MeV) produced by the activation of cobalt impurity of 1 gram. The comparison of the results in Table 4 indicates that even if the flux scaling factors are considered for the activation analysis, the gamma intensity produced by the activation per unit mass of cobalt impurity in the gas plenum and the bottom grid assembly could be larger than that produced in the active fuel node. Since the flux scaling factor of 1.0 and the relatively larger proportion of the thermalized neutrons compared to

the active fuel node were applied for the activation analysis of the bottom grid assembly, the gamma intensity produced per unit mass of cobalt impurity in the bottom grid assembly was estimated to be the strongest among the 6 nodes.

In terms of shielding analysis for a cask considering the effect of the activation source terms, the activation source of the assembly hardware is expected to have the greatest impact on a cask shielding model which has the maximum dose rate at upper or lower part of the cask side when considering the axial positions of the grid assemblies made of Inconel and the upper/lower end fitting made of stainless steel.

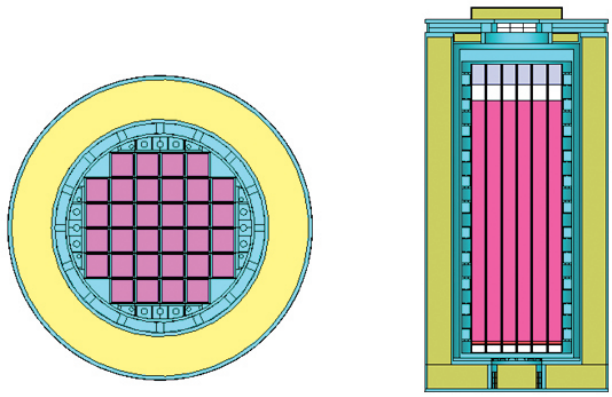

Fig. 5. Cross-sectional view (X-Y and X-Z planes) of the shielding model for OASIS-STO.

Table 5. Neutron source spectrum of active fuels for PLUS7 (Unit: n·sec^{-1}·MTU^{-1})

Group	Energy (MeV)		Without impurities (A)	With impurities (B)	B/A
	Upper	Lower			
1	1.96×10^{1}	1.42×10^{1}	2.52×10^{4}	2.51×10^{4}	0.996
2	1.42×10^{1}	1.22×10^{1}	1.15×10^{5}	1.14×10^{5}	0.996
3	1.22×10^{1}	1.00×10^{1}	7.33×10^{5}	7.30×10^{5}	0.997
4	1.00×10^{1}	8.61×10^{0}	1.82×10^{6}	1.81×10^{6}	0.997
5	8.61×10^{0}	7.41×10^{0}	4.25×10^{6}	4.23×10^{6}	0.997
6	7.41×10^{0}	6.07×10^{0}	1.24×10^{7}	1.24×10^{7}	0.998
7	6.07×10^{0}	4.97×10^{0}	2.41×10^{7}	2.41×10^{7}	0.998
8	4.97×10^{0}	3.68×10^{0}	6.42×10^{7}	6.40×10^{7}	0.997
9	3.68×10^{0}	3.01×10^{0}	6.10×10^{7}	6.08×10^{7}	0.997
10	3.01×10^{0}	2.73×10^{0}	3.32×10^{7}	3.31×10^{7}	0.997
11	2.73×10^{0}	2.47×10^{0}	3.54×10^{7}	3.53×10^{7}	0.997
12	2.47×10^{0}	2.37×10^{0}	1.48×10^{7}	1.48×10^{7}	0.998
13	2.37×10^{0}	2.35×10^{0}	3.05×10^{6}	3.04×10^{6}	0.998
14	2.35×10^{0}	2.23×10^{0}	1.89×10^{7}	1.89×10^{7}	0.998
15	2.23×10^{0}	1.92×10^{0}	5.34×10^{7}	5.34×10^{7}	0.999
16	1.92×10^{0}	1.65×10^{0}	5.20×10^{7}	5.19×10^{7}	1.000
17	1.65×10^{0}	1.35×10^{0}	6.33×10^{7}	6.33×10^{7}	1.001
18	1.35×10^{0}	1.00×10^{0}	7.98×10^{7}	7.99×10^{7}	1.001
19	1.00×10^{0}	8.21×10^{-1}	4.21×10^{7}	4.22×10^{7}	1.001
20	8.21×10^{-1}	7.43×10^{-1}	1.84×10^{7}	1.84×10^{7}	1.001
21	7.43×10^{-1}	6.08×10^{-1}	3.14×10^{7}	3.14×10^{7}	1.001
22	6.08×10^{-1}	4.98×10^{-1}	2.48×10^{7}	2.48×10^{7}	1.001
23	4.98×10^{-1}	3.69×10^{-1}	2.75×10^{7}	2.75×10^{7}	1.000
24	3.69×10^{-1}	2.97×10^{-1}	1.42×10^{7}	1.42×10^{7}	1.000
25	2.97×10^{-1}	1.83×10^{-1}	2.00×10^{7}	2.00×10^{7}	1.000
26	1.83×10^{-1}	1.11×10^{-1}	1.04×10^{7}	1.04×10^{7}	0.999
27	1.11×10^{-1}	6.74×10^{-2}	5.05×10^{6}	5.04×10^{6}	0.999
28	6.74×10^{-2}	4.09×10^{-2}	2.43×10^{6}	2.43×10^{6}	0.998
29	4.09×10^{-2}	3.18×10^{-2}	6.92×10^{5}	6.91×10^{5}	0.998
30	3.18×10^{-2}	2.61×10^{-2}	3.89×10^{5}	3.88×10^{5}	0.998
31	2.61×10^{-2}	2.42×10^{-2}	1.21×10^{5}	1.21×10^{5}	0.998
32	2.42×10^{-2}	2.19×10^{-2}	1.40×10^{5}	1.40×10^{5}	0.998
33	2.19×10^{-2}	1.50×10^{-2}	3.77×10^{5}	3.76×10^{5}	0.998
34	1.50×10^{-2}	7.10×10^{-3}	3.34×10^{5}	3.33×10^{5}	0.998
35	7.10×10^{-3}	3.35×10^{-3}	1.09×10^{5}	1.09×10^{5}	0.998
36	3.35×10^{-3}	1.58×10^{-3}	3.54×10^{4}	3.54×10^{4}	0.998
37	1.58×10^{-3}	4.54×10^{-4}	1.44×10^{4}	1.43×10^{4}	0.998
38	4.54×10^{-4}	2.14×10^{-4}	1.77×10^{3}	1.77×10^{3}	0.998
39	2.14×10^{-4}	1.01×10^{-4}	5.73×10^{2}	5.71×10^{2}	0.998
40	1.01×10^{-4}	3.73×10^{-5}	2.13×10^{2}	2.13×10^{2}	0.998
41	3.73×10^{-5}	1.07×10^{-5}	5.21×10^{1}	5.20×10^{1}	0.998
42	1.07×10^{-5}	5.04×10^{-6}	6.38×10^{0}	6.36×10^{0}	0.997
43	5.04×10^{-6}	1.86×10^{-6}	2.36×10^{0}	2.36×10^{0}	0.997
44	1.86×10^{-6}	8.76×10^{-7}	4.63×10^{-1}	4.61×10^{-1}	0.997
45	8.76×10^{-7}	4.14×10^{-7}	1.49×10^{-1}	1.49×10^{-1}	0.997
46	4.14×10^{-7}	1.00×10^{-7}	6.33×10^{-2}	6.31×10^{-2}	0.997
47	1.00×10^{-7}	1.00×10^{-11}	8.51×10^{-3}	8.48×10^{-3}	0.996
Total			7.21×10^{8}	7.20×10^{8}	0.999

Table 6. Gamma source spectrum of active fuels for PLUS7 (Unit: $\gamma \cdot sec^{-1} \cdot MTU^{-1}$)

Group	Energy (MeV)		Without impurities (A)	With impurities (B)	B/A
	Upper	Lower			
1	1.40×10^{1}	1.00×10^{1}	4.33×10^{4}	4.31×10^{4}	0.996
2	1.00×10^{1}	8.00×10^{0}	5.91×10^{5}	5.89×10^{5}	0.996
3	8.00×10^{0}	7.00×10^{0}	1.32×10^{6}	1.31×10^{6}	0.996
4	7.00×10^{0}	6.00×10^{0}	3.92×10^{6}	3.90×10^{6}	0.996
5	6.00×10^{0}	5.00×10^{0}	1.17×10^{7}	1.16×10^{7}	0.996
6	5.00×10^{0}	4.00×10^{0}	3.47×10^{7}	3.45×10^{7}	0.996
7	4.00×10^{0}	3.00×10^{0}	1.99×10^{9}	1.99×10^{9}	0.999
8 [1]	**3.00×10^{0}**	**2.00×10^{0}**	**1.37×10^{11}**	**1.49×10^{11}**	**1.089**
9	2.00×10^{0}	1.50×10^{0}	3.92×10^{12}	3.92×10^{12}	1.000
10 [2]	**1.50×10^{0}**	**1.00×10^{0}**	**1.19×10^{14}**	**3.35×10^{14}**	**2.819**
11	1.00×10^{0}	8.00×10^{-1}	8.25×10^{13}	8.24×10^{13}	1.000
12	8.00×10^{-1}	7.00×10^{-1}	3.36×10^{14}	3.36×10^{14}	0.999
13	7.00×10^{-1}	6.00×10^{-1}	3.95×10^{15}	3.95×10^{15}	1.000
14	6.00×10^{-1}	4.00×10^{-1}	1.80×10^{14}	1.80×10^{14}	1.001
15	4.00×10^{-1}	2.00×10^{-1}	2.14×10^{14}	2.14×10^{14}	1.001
16	2.00×10^{-1}	1.00×10^{-1}	4.41×10^{14}	4.42×10^{14}	1.001
17	1.00×10^{-1}	6.00×10^{-2}	4.37×10^{14}	4.38×10^{14}	1.001
18	6.00×10^{-2}	3.00×10^{-2}	1.02×10^{15}	1.02×10^{15}	1.001
19	3.00×10^{-2}	2.00×10^{-2}	5.00×10^{14}	5.02×10^{14}	1.003
20	2.00×10^{-2}	1.00×10^{-2}	1.06×10^{15}	1.06×10^{15}	1.002
Total			8.35×10^{15}	8.57×10^{15}	1.026

[1] Gamma intensity of Group 8 is considerably increased due to ^{208}Tl.

[2] Gamma intensity of Group 10 is considerably increased due to ^{60}Co.

Table 7. Axial distribution of neutron and gamma sources for PLUS7

Group	Node height (cm)	Neutron ($n \cdot sec^{-1}$)	Gamma ($\gamma \cdot sec^{-1}$)
1	381.00	2.87×10^{4}	2.19×10^{13}
2	371.95	9.08×10^{4}	2.23×10^{13}
3	365.76	3.55×10^{5}	1.67×10^{13}
4	362.90	2.39×10^{6}	6.76×10^{13}
5	352.90	5.32×10^{6}	8.17×10^{13}
6	342.90	1.80×10^{7}	1.86×10^{14}
7	322.90	2.12×10^{7}	1.80×10^{14}
8	304.80	2.37×10^{7}	1.85×10^{14}
9	286.70	2.61×10^{7}	2.05×10^{14}
10	266.70	2.61×10^{7}	2.05×10^{14}
11	246.70	2.37×10^{7}	1.85×10^{14}
12	228.60	2.37×10^{7}	1.85×10^{14}
13	210.50	2.61×10^{7}	2.05×10^{14}
14	190.50	2.61×10^{7}	2.05×10^{14}
15	170.50	2.37×10^{7}	1.85×10^{14}
16	152.40	2.37×10^{7}	1.85×10^{14}
17	134.30	2.61×10^{7}	2.05×10^{14}
18	114.30	2.61×10^{7}	2.05×10^{14}
19	94.30	2.37×10^{7}	1.85×10^{14}
20	76.20	2.20×10^{7}	1.82×10^{14}
21	58.10	2.02×10^{7}	1.92×10^{14}
22	38.10	6.40×10^{6}	8.55×10^{13}
23	28.10	3.19×10^{6}	7.23×10^{13}
24	18.10	4.67×10^{5}	1.77×10^{13}
25	15.24	1.25×10^{5}	2.40×10^{13}
26	9.05	3.24×10^{4}	2.27×10^{13}

On the other hand, notable elements (or nuclides) for the radiation source among the impurities in the fuel listed in Table 2 are cobalt, thorium and the light elements. The cobalt impurity of 75 ppm in the fuel could produce considerable gamma source by activation during reactor power operation. For the thorium impurity, natural abundance of 100% ^{232}Th was assumed. ^{232}Th itself is not a strong gamma emitter, but it has very long half-life of 1.41×10^{4} million years and some nuclides in the decay chain of ^{232}Th may have considerable effect on the gamma source for shielding analysis, especially after the spent fuel cooling for several years. For example, ^{208}Tl is one of the nuclides in the decay chain and emits a high energy decay gamma of 2.61 MeV with 99.8% probability. Oxygen is the principal light element which produces (α,n) neutrons in UO_2 fuel but other light elements in Table 2 could also slightly increase the (α,n) neutron emission intensity. However, the effect of the impurities in the fuel on the neutron intensity is expected to be much smaller than the effect on the gamma intensity.

2.3 Shielding

Fig. 5 shows cross-sectional view (X-Y and X-Z planes) for the shielding model of OASIS-STO. OASIS-STO is a

Table 8. Specification for OASIS-STO

Dimensions		
Height of cask		6,030 mm
Outer diameter of cask		2,875 mm
Height of canister		4,770 mm
Outer diameter of canister		1,785 mm
Thickness of high density concrete shield (radial)		375 mm
Thickness of carbon steel shield (radial)		35 mm
Thickness of neutron absorber		3.5 mm
Weights		
Cask including canister with fuel unloaded		97 tons
Cask including canister with maximum fuel loaded		118 tons
Materials		
Fuel assembly (PLUS7)	- UO_2	• Fuel pellet
	- ZIRLO	• Fuel cladding • Guide thimble • Mid grid assembly
	- Inconel-718	• Top/Bottom grid assembly • Protective grid assembly
	- SS304	• Upper/Lower end fitting
Cask body	- High density concrete (Density: 3.62 $g \cdot cm^{-3}$)	
Cask shell	- Carbon steel (iron: 99wt%, carbon: 1wt%)	
Canister	- Stainless steel (SS304)	
Baskets	- Stainless steel (SS304)	
Neutron absorber	- MAXUS (aluminum: 60wt%, B_4C: 40wt%)	

dry storage cask which has four air inlets at lower part of the cask side and four outlets at upper part of the cask side. The air inlets and outlets are essential for dry storage casks with natural convection cooling systems, however, the air flow path is bound to be a weak point in terms of radiation shielding.

In order to investigate the effect on the radiation shielding of a cask depending on whether the impurities of Tables 1 and 2 are taken into account, the shielding analysis model of OASIS-STO was chosen and the SCALE/MAVRIC module was used. For a case of the shielding analysis which does not consider the impurities, the active fuels with 381 cm height excluding other structural regions were modeled only, for conservatism. The neutron and gamma source spectrum of the active fuel per each PLUS7 fuel assembly is shown in Tables 5 and 6, respectively. Total gamma activity for each node was calculated based on the activation source produced by cobalt impurity of 1 gram in Table 4, considering the total mass of cobalt impurity in each node. The axial distribution of neutron and gamma sources derived from axial power distribution for PLUS7 [4] is shown in Table 7. Mesh tally was used for the MAVRIC evaluation and the mesh region was set over the cask side surface of azimuthal angles for 45 and 90 degrees. The mesh region of the inlet surface was evaluated separately from the rest of the cask side taking into account the complex geometries and the expected large uncertainties. The mesh region for the air inlet was set from 45.75 to 145.75 cm by radial distance through the air inlet path for the 45 degree. The specification for OASIS-STO such as dimension, material and etc. is shown in Table 8. Flux-to-dose-rate conversion factors of ANSI-6.1.1-1977 were applied to the evaluation, as recommended in NUREG-2215 [5].

3. Results

The evaluated dose rate distribution on the cask side surface for azimuthal angles of 45 and 90 degrees excluding the inlet area is shown in Figs. 6 and 7, respectively. The mid-height of the active fuel was set to zero (cm) for the axial distribution. The neutron and gamma dose rates for the 45 degree were evaluated to be generally larger than those for the 90 degree because the cask side surface for the 45 degree is closer to the outer edge for the source region of the 32 assemblies in the cask; moreover, the reinforcement supports made of stainless steel installed at the azimuthal angles of 0, 90, 180 and 270 degrees inside the canister serve as a shield.

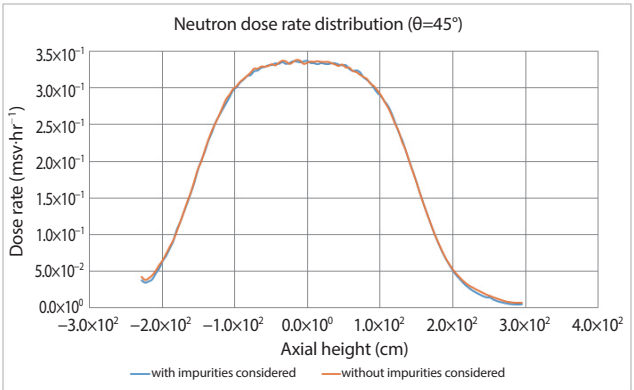

Fig. 6. Dose rate distribution of cask side surface for azimuthal angle of 45 degree.

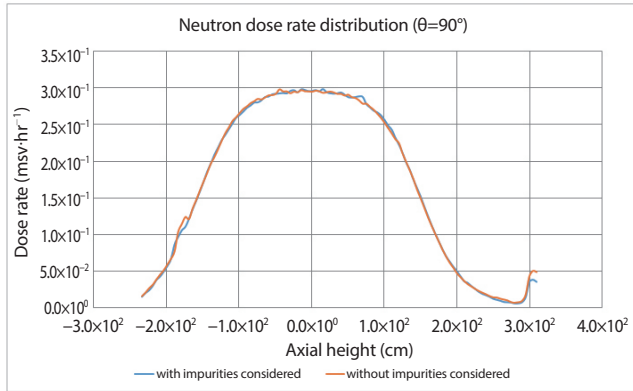

Fig. 7. Dose rate distribution of cask side surface for azimuthal angle of 90 degree.

Whether or not the impurities are considered did not significantly affect the neutron does rates. However, the gamma dose rates were evaluated to be considerably increased when the impurities were considered. It was estimated that the gamma dose rates from the active fuel could increase by about two times when the impurities are considered. Especially, the gamma dose rate from the gas plenum (190.5–215.9 cm height) was estimated to be the greatest among the 6 nodes. The maximum gamma dose rate for the case considering the impurities was estimated to be 0.606 mSv·hr^{-1} at the medium height of the gas plenum. This is because the total gamma intensity from the ^{60}Co produced by the activation in the gas plenum node is the largest among the 6 nodes. The gas plenum node includes not only the top grid assembly made of Inconel but the springs made of SS302 inside the fuel rods also. The cobalt impurity concentration for SS302 was assumed to be the same with SS304 in the gas plenum activation analysis. The average relative uncertainty of the estimated dose rates for the mesh region of the cask side surface was estimated to be less than 5% for both neutrons and gammas.

The evaluated dose rate distribution for the air inlet path is shown in Fig. 8. A logarithmic scale was used for the y-axis of the graph in Fig. 8. Whether or not the impurities are considered did not significantly affect the neutron dose rates but the case excluding the impurities showed slightly larger neutron dose rates. It is estimated that this is because the active fuel node excluding the other assembly hardware regions was only modeled as the source region for the case without considering the impurities. And, unlike uranium, some of the impurity elements in Table 2 would capture the neutrons without neutron multiplication by fission. For the

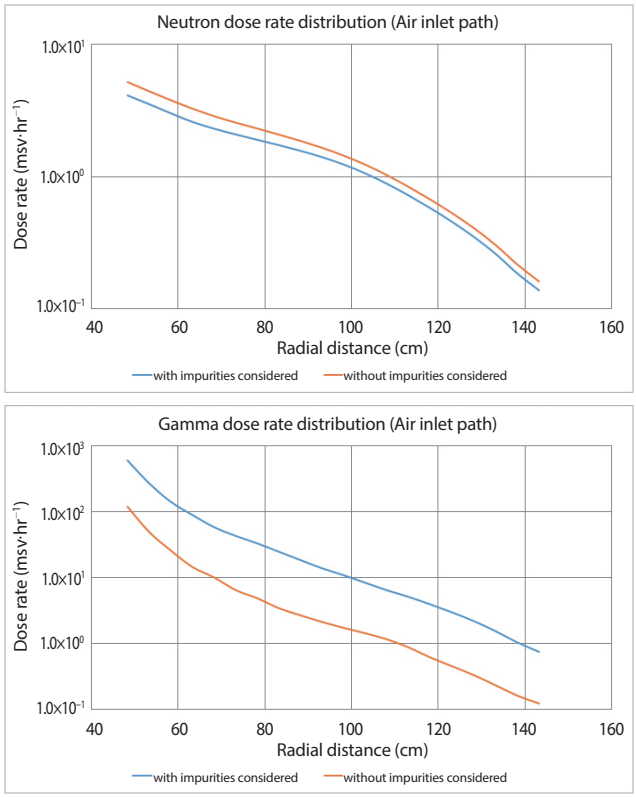

Fig. 8. Dose rate distribution of the air inlet path (45 degree).

gamma dose rates, the effect of the considered impurities was estimated to be considerable. The gamma dose rate at the center of the air inlet on the cask side surface was evaluated to be 0.124 $mSv \cdot hr^{-1}$ for the case without considering the impurities and 0.742 $mSv \cdot hr^{-1}$ for the case considering the impurities, respectively. This increment would be caused mainly by the activation source of the lower end fitting for the case considering the impurities. The average relative uncertainty of the estimated dose rates for the mesh region of the air inlet path was estimated to be less than 10% for both neutrons and gammas.

4. Conclusions

The effect of the impurities in the fuel and structural materials on the radiation source term and shielding was evaluated based on the generic storage cask model and the conservative assumption on the impurity concentration. The assumed impurity concentration was based on the maximum value provided in the publicly available research data. Thus, the results of the case considering the impurities in this study may include substantial safety margin in terms of the shielding, but anyway, it seems that the cobalt among the considered impurities would have the greatest impact on the shielding and should be adequately considered for a conservative and safe shielding design. Due to the wide range of potential cobalt impurity concentration for UO_2 fuel and Inconel, determination of concentration values which are appropriate for the activation analysis would be important according to analysis purpose. Also, the impact of thorium impurity may not be negligible for a particular shielding model where the high energy gamma of 2.61 MeV from ^{208}Tl is important. The light element impurities such as boron, carbon, nitrogen and etc. which increase the (α,n) neutron emission intensity could be considered for conservatism but their impact on the neutron source would be not so significant. The other elements of the impurities in Table 2 seem to have negligible effect and they may be excluded in the analysis.

For the activation of the structural materials, it was estimated that the gas plenum region could be the strongest gamma source region for the shielding model for the cask side surface. This is because the total mass of cobalt impurities in the top grid assembly and the springs inside the fuel rods of the gas plenum region is the second largest among the 6 nodes and the cross section for $^{59}Co(n,\gamma)$ reaction was estimated to be the largest in the gas plenum. As described above, the gas plenum region could include the greatest gamma intensity due to the ^{60}Co and the axial height range of the gas plenum is relatively small, thus the gamma sources become compact in the gas plenum region. Consequently, the maximum gamma dose rate is shown around the height of 200 cm where the gas plenum is located.

Since the impurity concentration limits specified in the material standards cannot fully cover all possible elements

actually present in fuel and structural materials, various experimental data and studies will be required for a more valid and appropriate evaluation for design application.

Acknowledgements

This work was supported by the Korea Institute of Energy Technology Evaluation and Planning (KETEP) and the Ministry of Trade, Industry & Energy (MOTIE) of the Republic of Korea (No. 2021171020001A).

REFERENCES

[1] W.A. Wieselquist, R.A. Lefebvre, and M.A. Jessee. SCALE Code System, Oak Ridge National Laboratory Technical Report, ORNL/TM-2005/39, Version 6.2.4 (2020).

[2] A. Luksic. Spent Fuel Assembly Hardware: Characterization and 10CFR 61 Classification for Waste Disposal, Volume 1: Activation Measurements and Comparison With Calculations for Spent Fuel Assembly Hardware, Pacific Northwest Laboratory Report, PNL-6906 Vol. 1 Report (1989).

[3] S. Häkkinen. Impurities in LWR Fuel and Structural Materials, VTT Technical Research Center of Finland Report, VTT-R-00184-20 (2020).

[4] KEPCO Engineering & Construction Company Inc. Development of Technology and Models on Casks for Spent Nuclear Fuel, KEPCO E&C Final Report, KEPCO E&C/21-TNA66-01 (2021).

[5] United States Nuclear Regulatory Commission. Standard Review Plan for Spent Fuel Dry Storage Systems and Facilities, U.S. NRC Final Report, Chapter 6 30-31, NUREG-2215 (2020).